2-22-2018

An Empirical Model for Estimating Soil Thermal Diffusivity from Texture, Bulk Density, and Degree of Saturation

Xiaoting Xie
China Agricultural University

Yili Lu
China Agricultural University

Tusheng Ren
China Agricultural University

Robert Horton
Iowa State University, rhorton@iastate.edu

An Empirical Model for Estimating Soil Thermal Diffusivity from Texture, Bulk Density, and Degree of Saturation

Abstract

Soil thermal diffusivity κ is an essential parameter for studying surface and subsurface heat transfer and temperature changes. It is well understood that κ mainly varies with soil texture, water content θ, and bulk density ρ_b, but few models are available to accurately quantify the relationship. In this study, an empirical model is developed for estimating κ from soil particle size distribution, ρ_b, and degree of water saturation S_r. The model parameters are determined by fitting the proposed equations to heat-pulse κdata for eight soils covering wide ranges of texture, ρ_b, and S_r. Independent evaluations with published κdata show that the new model describes the $\kappa(S_r)$ relationship accurately, with root-mean-square errors less than 0.75×10^{-7} m^2 s^{-1}. The proposed $\kappa(S_r)$ model also describes the responses of κ to ρ_b changes accurately in both laboratory and field conditions. The new model is also used successfully for predicting near-surface soil temperature dynamics using the harmonic method. The results suggest that this model provides useful estimates of κ from S_r, ρ_b, and soil texture.

Disciplines

Agricultural Science | Hydrology | Soil Science | Statistical Models

Comments

This is a manuscript of an article published as Xie, Xiaoting, Yili Lu, Tusheng Ren, and Robert Horton. "An empirical model for estimating soil thermal diffusivity from texture, bulk density, and degree of saturation." *Journal of Hydrometeorology* (2018). doi: 10.1175/JHM-D-17-0131.1. Posted with permission.

AMERICAN METEOROLOGICAL SOCIETY

Journal of Hydrometeorology

EARLY ONLINE RELEASE

The DOI for this manuscript is doi: 10.1175/JHM-D-17-0131.1

An empirical model for estimating soil thermal diffusivity from texture, bulk density, and degree of saturation

XIAOTING XIE

Department of Soil and Water Sciences, China Agricultural University, Beijing, China

YILI LU

Department of Soil and Water Sciences, China Agricultural University, Beijing, China

TUSHENG REN

Department of Soil and Water Sciences, China Agricultural University, Beijing, China

ROBERT HORTON

Department of Agronomy, Iowa State University, Ames, Iowa

Corresponding author address: Yili Lu, Department of Soil and Water Sciences, China Agricultural University, Beijing, China 100193

Email: luyili@cau.edu.cn

ABSTRACT

Soil thermal diffusivity (κ) is an essential parameter for studying surface and subsurface heat transfer and temperature changes. It is well understood that κ mainly varies with soil texture, water content (θ), and bulk density (ρ_b), but few models are available to accurately quantify the relationship. In this study, an empirical model is developed for estimating κ from soil particle size distribution, ρ_b, and the degree of water saturation (S_r). The model parameters are determined by fitting the proposed equations to heat-pulse κ data for eight soils covering wide ranges of texture, ρ_b and S_r. Independent evaluations with published κ data show that the new model describes the $\kappa(S_r)$ relationship accurately, with root mean square errors less than 0.75×10^{-7} m^2 s^{-1}. The proposed $\kappa(S_r)$ model also describes the responses of κ to ρ_b changes accurately in both laboratory and field conditions. The new model is also used successfully for predicting near-surface soil temperature dynamics using the harmonic method. The results suggest that this model provides useful estimates of κ from S_r, ρ_b and soil texture.

1. Introduction

Soil thermal diffusivity (κ) describes the speed of soil temperature wave transmission and determines the depth of soil influenced by diurnal surface heating and cooling. Knowledge of κ is essential for modeling coupled heat and water transfer in soils and ground energy budgets, and for predicting soil temperature in land surface models (Xia et al. 2013; Koch et al. 2016). Furthermore, κ has been used for estimating soil heat flux (de Silans et al. 1996; Roxy et al. 2014), an important component of land surface energy balance that influences the energy exchange between land surface and the atmosphere (Heusinkveld et al. 2004).

Only a few methods are available for measuring κ directly. The surface step change in temperature method, which estimates κ using the analytical solution to the one-dimensional heat conduction equation (Jackson and Taylor 1986; Horton 2002), works only on laboratory soil columns. Recently, heat pulse (HP) probes have been accepted as reliable tools for in situ measurement of soil thermal properties. A heat pulse is introduced into the soil, and κ is determined from the temperature changes at a distance from the heater according to the pulsed line heat source theory (Bristow et al. 1994; Kluitenberg et al. 1995; Liu et al. 2017). The small sampling volume and relatively sophisticated equipment setup, however, limit the extensive application of the HP technique in field conditions. An infrared thermal imaging technique has also been proposed for determining field κ values, but is limited to the soil surface layers (Kodikara

et al. 2011).

Numerous studies have focused on determination of apparent κ from periodic (diurnal or annual) temperature measurements at multiple depths. Most of the temperature-based approaches use analytical solutions to the heat transfer equation with sinusoidal or Fourier-series upper temperature boundary conditions (Carslaw and Jaeger 1959), assuming a uniform soil profile with conduction as the dominant heat transfer mode (Horton 2002). Among these, the amplitude, phase (Van Wijk and de Vries 1963; Wierenga et al. 1969), arctangent (Nerpin and Chudnovskii 1967) and logarithmic (Seemann 1979) methods, which have explicit forms and use small numbers of temperature data, tend to produce inconsistent or erroneous κ values near the soil surface where the temperature dynamics differ from sine-wave curves or two-harmonic functions (Horton et al. 1983). The numerical and harmonic methods, which make use of large numbers of temperature observations to implicitly solve for κ values, provide more reliable estimates (Richtmeyer and Mortor 1967; Horton et al. 1983). Evett et al. (2012) reported that the harmonic method-based κ and de Vries (1963) model-based soil volumetric heat capacity (C) led to better surface heat flux estimates than measurements with heat flux plates. Nonetheless, like other temperature-based methods, the κ results from the numerical and harmonic methods are unable to capture the spatial and temporal variations of κ (e.g., at various soil depths during wetting/drying periods). Some researchers developed analytical (Lettau 1954) and numerical (Nassar and Horton 1989,

70 1990) solutions for estimating κ of nonuniform soils. These approaches usually fail when
71 an abrupt change occurs in the temperature wave, which can happen during or just after a
72 rainfall event (de Silans et al. 1996). Ross (2013) proposed a Fourier analysis for
73 estimating κ by considering in-depth θ variations and the effects of transient terms. The
74 method, which is relatively complicated and requires soil temperature observations at
75 several depths, has not been applied widely to field conditions.

76 In meteorological and geophysical applications, κ is estimated frequently using soil
77 thermal property models that relate soil thermal conductivity (λ) and C to volume
78 fractions of the soil particles, θ, and soil bulk density (ρ_b) (Wang and Bou-Zeid 2012;
79 Holmes et al. 2008). These models, either empirical (Johansen 1975; McCumber and
80 Pielke 1981; Campbell 1985) or physically based (de Vries 1963), have provided valuable
81 tools for simulating thermal and hydraulic processes that relate to climate change and
82 geophysical flows. However, many studies have demonstrated that the λ models are often
83 subject to errors caused by empirical parameters and to ignoring λ variability over space
84 and time, which result in misleading κ results, and therefore, problematic soil
85 temperature and heat flux estimations (Gao et al. 2017a). For example, the Johansen
86 (1975) λ model has been reported to produce erroneous soil heat flux estimates, because
87 it is sensitive to soil porosity and quartz content (Peters-Lidard et al. 1998). Lu et al.
88 (2007) showed that although the Johansen (1975) λ model was suitable for
89 coarse-textured soils, it underpredicted λ for the entire θ range on fine-textured soils. The

McCumber and Pielke (1981) λ model, which has been used widely in modeling land surface processes, overestimates λ during wetting and underestimates λ during drying, thus leads to errors in surface heat fluxes (Peters-Lidard et al. 1998). For this reason, some researchers arbitrarily set an upper λ limit of 1.9 W m^{-1} K^{-1} (Chen and Dudhia 2001). The five model parameters in the Campbell (1985) λ model vary with soil organic matter (SOM), texture, ρ_b and θ, making it difficult to determine λ accurately. Bristow (1998) showed that inaccurate quartz contents in the Campbell (1985) λ model led to more than 4°C errors in soil temperature predictions.

As an intrinsic soil property, κ is affected by soil mineral composition, porosity, particle arrangement, soil texture and temperature (Ochsner et al. 2001; Roxy et al. 2014), and varies nonlinearly with θ (Campbell 1985). For most mineral soils, κ increases quickly as dry soil wets, reaches the maximum value at a certain θ, and then decreases slowly as θ continues to increase (Ren et al. 1999; Wang et al. 2005; Liu et al. 2008a; Guan et al. 2009; Roxy et al. 2014). Under field conditions, κ shows strong temporal and spatial variability due to changes in θ and ρ_b with depth and time (Gao et al. 2017b). In practice, however, κ is often assumed constant with depth and time when estimating soil heat flux (Wang and Bou-Zeid 2012; Russel et al. 2015). Arkhangel'skaya (2009) used a lognormal function to describe the dependence of κ on θ for relatively fine-textured soils with sand fractions (f_{sa}) less than 0.40. On coarse-textured soils, however, the lognormal function produced large errors. Thus, there is a need for a model that estimates κ with

readily-available physical parameters for applications on various soil types over a range of field conditions.

The objective of this study is to develop an empirical model that is able to describe κ as a function of soil texture, ρ_b and degree of saturation (S_r). The performance of the model is evaluated by comparing estimated κ values with independent κ measurements using the HP method under both laboratory and field conditions. The new κ model is applied in the conduction heat transfer equation to estimate subsurface soil temperature from harmonic surface temperature. The estimated subsurface temperatures are compared to measured soil temperatures.

2. Datasets for model development and validation

In this study, the $\kappa(S_r)$ data were obtained under laboratory (Soils 1-15) and field conditions (Soil 16) covering a wide range of soil texture, ρ_b, and θ. Table 1 lists the particle size distribution (PSD), SOM content and ρ_b range for the soil samples and the data sources. Soil PSD was determined using the pipette method (Gee and Or 2002), and SOM content was determined using the Walkley-Black titration method (Nelson and Sommers 1996). Soils 1-8, with f_{sa} ranging from 19% to 94%, were used to develop the κ model. Soils 9-16, with f_{sa} varying from 12% to 93%, were used to validate the model.

2.1 κ measurements on repacked soil samples

For Soils 1-8, samples were air-dried, ground and sieved through a 2-mm screen, moistened to the desired water contents, repacked into columns with a volume of 100 cm^3

130 (5-cm diameter and 5-cm high), sealed with plastic sheets, and then equilibrated in a
131 room at regulated temperature (20 ± 1°C) for 24 h. Soil thermal property measurements
132 were made with a three-needle HP sensor that was inserted into each soil column
133 vertically. The three-needle HP sensor consisted of three parallel stainless-steel needles
134 with 1.3-mm in diameter, 40-mm in length and 6-mm in probe spacing between the
135 heater and sensor probes. The heater probe contained a resistance wire in the heater probe,
136 and a chromel-constantan thermocouple centered in the middle of the three probes for
137 measuring temperature (Ren et al. 1999; Lu et al. 2017). The HP measurements were
138 controlled with a data logger (CR23X, Campbell Scientific, Logan, UT). A 15-s HP was
139 supplied to the heater probe by using a direct current power supply. The datalogger
140 recorded the power input and temperature change of the sensor probe at a 1-s interval.
141 The temperature-by-time data were processed to calculate κ using the nonlinear
142 regression algorithm of Welch et al. (1996). The final κ was the mean value of three
143 repeated measurements. Gravimetric θ and ρ_b of each soil core were determined after
144 making the HP measurements. Before making the HP measurements, the needle-to-needle
145 spacing of the three-needle HP sensor was calibrated in agar-stabilized water (5 g L^{-1}),
146 assuming that the C of the solution was equal to that of water (4.18 MJ m^{-3} K^{-1}).

147 Thermal properties for Soils 9, 14, and 15 were reported in Liu et al. (2008b) who
148 made HP measurements on repacked soil cores with various θ and ρ_b. Thermal properties
149 for Soils 10-13, with a wide range of ρ_b and θ on repacked samples were reported in

Ochsner et al. (2001). Refer to Liu et al. (2008b) and Ochsner et al. (2001) for the details of the sample preparation and the HP measurements for obtaining κ.

2.2 κ measurements in field tillage plots

Field measurements were performed on a silt loam soil (Soil 16) at the Luancheng Agricultural Ecosystem Experimental Station of the Chinese Academy of Sciences, Hebei, China. Three contrasting tillage systems were included in the study: Conventional moldboard plow tillage (CT), rotary tillage (RT), and no tillage (NT). For CT and RT, all crop residue was chopped into small pieces (5- to 10-cm long) and then incorporated into the soil after corn harvest. The tillage depth for the CT and RT was about 18 cm and 12 cm, respectively. More than 95% of the surface residue was mixed into the soil. For NT, standing corn stubble was left on the ground surface, and the soil was not disturbed before planting. The amount of returned crop residue was 9.2, 9.2 and 8.5 Mg ha^{-1} yr^{-1} for CT, RT and NT, respectively. After winter wheat harvest in June 2007, in situ HP measurements were made in each tillage plot at three random locations. Four repeated κ measurements were performed at each location. Before installing the HP sensors, a small trench (20-cm long, 20-cm wide and 20-cm deep) was dug, and two three-needle HP sensors were pushed horizontally into the soil at depths of 5 cm and 15 cm. The HP data were collected with a datalogger (CR23X, Campbell Scientific, Logan, UT). Undisturbed soil columns were collected nearby with ring samplers (5-cm diameter and 5-cm high) at soil depths of 5 and 15 cm to determine ρ_b and θ by oven-drying the samples at 105°C for

24 h.

2.3 Near-surface temperature measurement and prediction

To test the model performance, we measured soil temperature on a bare sandy loam soil (79.8% sand and 12.3% clay) at the research farm of China Agricultural University, Beijing, China. Three-wire thermocouples (type E, 50 μm in diameter), which were embedded in stainless-steel needles (4 cm long, and 1.3 mm in diameter), were installed at 14-, 26-, and 66-mm depths, and soil temperatures were recorded at an 1-h interval with a datalogger (CR23X, Campbell Scientific, Logan, UT) during a rain-free period from day of year (DOY) 258 to 264 in 2014. The ρ_b values of the 0- to 50-mm and 50- to 100-mm soil layers were measured with a core sampler (5-cm diameter and 5-cm high) on DOY 258, 260, and 263. Since ρ_b did not vary over time during the observation period, the mean ρ_b values (from 3 repeated measurements) of 1.29 g cm^{-3} and 1.36 g cm^{-3} were used for the 0- to 50-mm layer and 50- to 100-mm layer, respectively. Hourly θ measurements at the 20- and 60-mm depths were recorded automatically with a time domain reflectometer (TDR100, Campbell Scientific, Logan, UT). Three TDR probes were installed at each depth. The net radiation data were recorded at a 1-h interval with two net radiometers (AV-71NR, Avalon Scientific, Jersey City, NJ) mounted at 0.1 m above the soil surface. Refer to Peng et al. (2017) for the details the of field experiment setup.

We applied the harmonic method to predict soil temperature changes at the 26- and

66-mm depths using measured temperatures at the 14-mm depth (boundary temperature) and κ estimates from the new model (Horton et al. 1983). For a uniform soil with the surface subjected to a periodic temperature wave, the daily upper boundary soil temperature dynamics can be described with a Fourier series (Horton et al. 1983),

$$T(0,t) = \overline{T} + \sum_{n=1}^{M}\left[A_n \sin\left(n\omega t + \phi_n\right)\right], \quad [1]$$

where $\overline{T}$ is the average surface temperature for each day (°C), t represents time (h), M is the number of harmonics, A_n and ϕ_n are the amplitude and phase angle of the n^{th} harmonic, respectively, ω is the radial frequency equal to $2\pi/P$ with P being the period of the fundamental cycle (24 h for daily temperature). Accordingly, based on the heat conduction equation with M harmonics as boundary condition, the temperature at a depth z (m) below the upper boundary depth is approximated by (Horton et al. 1983),

$$T(z,t) = \overline{T} + \sum_{n=1}^{M}\left[A_n \exp\left(-z\sqrt{n\omega/2\kappa}\right)\sin\left(n\omega t + \phi_n - z\sqrt{n\omega/2\kappa}\right)\right]. \quad [2]$$

In our study, Eq. [1] was applied to fit the observed boundary temperatures at 14-mm depth, and Eq. [2] was applied to predict subsurface temperatures at depths 26 mm and 66 mm with model-derived κ data. The reliability of the κ model was then evaluated by comparing the measured and predicted temperatures at the two soil depths.

3. Model development

3.1 The empirical soil κ model

According to the linear mixing model, C is expressed as the sum of heat capacities

209 of water and soil solids (de Vries 1963; Campbell 1985),

210 $$C = \rho_b c_s + \rho_w c_w \theta, \quad [3]$$

211 where c_w is specific heat of water (4.18 J g^{-1} k^{-1}), and ρ_w is the density of water (1.0 g

212 cm^{-3}).

213 Lu et al. (2014) present an empirical model that relates λ to θ, ρ_b and texture,

214 $$\lambda = \exp(\beta - \theta^{-\alpha}) + \lambda_{dry} \qquad \theta > 0, \quad [4]$$

215 where α and β are shape factors related to ρ_b and PSD, and λ_{dry} is the thermal

216 conductivity of dry soils that can be estimated from soil porosity (τ).

217 In this study, we take the forms of the de Vries (1963) C model and the Lu et al.

218 (2014) λ model to establish a general model that estimates κ from other soil physical

219 properties. As the ratio of λ and C, κ is also a function of soil texture, θ and ρ_b. Instead of

220 using θ, we use the dimensionless parameter S_r, which makes it easy to make

221 comparisons between soils of different textures. We propose the following equation that

222 relates κ to soil PSD, ρ_b, and S_r,

223 $$\kappa(S_r) = \frac{0.25 + \exp(b - S_r^{-a})}{4.18 S_r + c} \qquad S_r > 0, \quad [5]$$

224 where *a*, *b* and *c* are the shape parameters of the $\kappa(S_r)$ curve, 4.18 (MJ m^{-3} K^{-1}) is the heat

225 capacity of water at room temperature (Campbell et al. 1991), and 0.25 (W m^{-1} K^{-1}) is

226 selected to represent the average λ_{dry} value for mineral soils of different textures (de

227 Vries 1963). Taking soil particle density as 2.65 g cm^{-3}, S_r is calculated from the ratio of θ

228 and τ.

Figure 1 illustrates the measured (dots) and the fitted (lines) κ-S_r results using Eq. [5] for Soils 1-8. Except for Soil 2, the S_r on the repacked soil samples ranged from about 0 to 1 (Table 2). In general, the measured $\kappa(S_r)$ data and fitted curves displayed several distinct features across soils. First, κ changed dynamically as dry soil wetted. In general, κ increased rapidly until S_r reached about 0.2. With further increases in S_r, however, the rate of κ change was reduced. After reaching a peak value (κ_m) at a certain S_r, κ either declined steadily (e.g., Soils 1-5) or leveled off (e.g., Soils 6-8) as S_r increased. Secondly, the magnitude and shape of the $\kappa(S_r)$ curves were strongly related to soil texture, i.e., with increasing S_r, κ_m was larger and occurred at lower S_r for coarse-textured soils, but was relatively lower and occurred at larger S_r for fine-textured soils. These phenomena can be explained by the fact that: (1) coarse soils (Soils 1–5) usually have more quartz content than fine soils, and the κ of quartz (4.13×10^{-7} m^2 s^{-1}) is much larger than that of other soil minerals (1.08×10^{-7} m^2 s^{-1}, Campbell and Norman 1998), leading to larger κ_m values for coarse soils than for fine soils; and (2) fine soils require more water to form water bridges between the solid particles, which leads to smaller changes in fine than in coarse soils in the λ-θ curve at the same S_r as dry soil initially wets (Ewing and Horton 2007; Lu et al. 2007), and thus relatively small changes in $\kappa(S_r)$. In addition, an increase in ρ_b results in a greater κ value at a specific S_r. This was illustrated for the case of Soil 2, where the increase in $\kappa(S_r)$ was found to be as large as 1.60×10^{-7} m^2 s^{-1} when ρ_b was changed from 1.28 to 1.49 g cm^{-3} for the repacked S_r range of 0.02-0.64. This observation

249 was consistent with the findings of Ochsner et al. (2001) who reported that κ decreased
250 linearly with air-porosity (that related inversely to ρ_b) on four loamy soils.

251 The coefficients of determination (R^2) for the fitted results were all greater than 0.99
252 (data not shown), and the root mean square error (RMSE) values were within 0.35×10^{-7}
253 $m^2\ s^{-1}$ for the eight soils (Table 2), indicating that the proposed model well described the
254 measured $\kappa(S_r)$ values across the entire S_r range.

255 *3.2 Determination of model parameters a, b, and c*

256 Our earlier analysis indicates that for a specific soil, the κ values are well-described
257 by S_r, PSD, and ρ_b, and the shape and magnitude of the $\kappa(S_r)$ curves are defined by
258 parameters *a*, *b* and *c*. In this section, we perform a sensitivity analysis to investigate how
259 *a*, *b* and *c* influence the $\kappa(S_r)$ curves, and then establish functional relationships among
260 these parameters versus PSD and ρ_b.

261 For Soils 1-8, parameters *a*, *b* and *c* varied in the ranges of 0.20–0.46, 4.27–5.35 and
262 1.28–5.45, respectively (Table 2). To examine the effects of *a* on the $\kappa(S_r)$ curve, we
263 assigned a value of 4.27 to *b* and a value of 5.45 to *c*, both corresponded to the lowest
264 fitted values of *b* and *c* (Table 2). Then parameter *a* was varied from 0.20 to 0.46, which
265 covered the fitted *a* range on Soils 1-8 (Table 2). Similarly, for examination of the effect
266 of parameter *b* on $\kappa(S_r)$ curve, we assigned a value of 0.46 to *a* and 5.45 to *c*, while *b*
267 varied from 4.27 to 5.35. To examine the effect of *c* on the $\kappa(S_r)$ curve, we set *a* at 0.46
268 and *b* at 4.27, while *c* varied from 1.30 to 5.50.

The effects of parameter a on the $\kappa(S_r)$ curve were pronounced in the relatively dry region ($S_r < 0.3$), while parameters b and c generally influenced the $\kappa(S_r)$ curve across the entire S_r range (Fig. 2). A higher a value produced a lower rate of $\kappa(S_r)$ increase in the relatively low S_r region (Fig. 2-1). With an increase of parameter c, the κ value at a specific S_r also decreased, especially in the intermediate S_r region (Fig. 2-3). An opposite trend was observed for parameter b, i.e., higher b values led to greater κ values, and the change of κ was especially significant in the high S_r region (Fig. 2-2). In general, the $\kappa(S_r)$ curve was more sensitive to parameter a in the low S_r region, to c in the intermediate S_r region, and to b in the high S_r region. For example, when a, b and c varied in the designated ranges, the maximum changes of κ were 1.80, 5.34 and 3.16×10^{-7} m^2 s^{-1}, respectively. At low θ values (i.e., the dry end of the $\lambda(\theta)$ curve), heat conduction occurs through soil solid particles where soil water exists mainly as water films around the solids (Lu et al. 2007; Lu et al. 2014). Soils with higher clay contents have larger surface areas, and thus, adsorb more water molecules around the solid particles, which leads to a gradual change in the $\lambda(\theta)$ curve in the low S_r region. At intermediate and high θ values, the magnitude of heat conduction through soil particles depends largely on the capillary bridges among solid particles, which are controlled by soil porosity and pore-size distribution. It appears that parameter a, which has significant effects on the $\kappa(S_r)$ curves in the low S_r region, is closely related to the soil clay fraction (f_{cl}). Parameters b and c

288 relate mainly to f_{sa} and ρ_b, the key factors that determine soil porosity and pore size
289 distribution, and thus the capillary bridges.

290 To quantify the dependence of parameters *a*, *b* and *c* on soil physical properties, we
291 further examined the relations among parameters *a*, *b* and *c* and PSD and ρ_b (Fig. 3). The
292 results showed that parameter *a* increased linearly with f_{cl}, and the rate of increase was
293 larger in the f_{cl} range of 0–0.12 than that in the range of $f_{cl} > 0.12$ (Fig. 3-1). Parameters *b*
294 and *c* depended largely on f_{sa}: with increasing f_{sa}, both *b* and *c* first decreased and then
295 increased with a splitting point of $f_{sa} = 0.40$ (Figs. 3-2 and 3-3). This is in line with the
296 findings of Johansen (1975) and Lu et al. (2007) who classified the fine-textured and
297 coarse-textured soils using a f_{sa} value of 0.40 in their λ models. Hereafter, we will
298 describe soils with $f_{sa} > 0.40$ as coarse-textured soils, and soils with $f_{sa} \leq 0.40$ as
299 fine-textured soils.

300 Based on the values listed in Table 2, we performed a linear regression analysis to
301 obtain the a-f_{cl} and c-f_{sa} relationships with piecewise functions,

302
$$\begin{cases} a = 3.06 f_{cl} + 0.05 & f_{cl} < 0.12 \quad R^2 = 0.86 \\ a = 0.83 f_{cl} + 0.20 & f_{cl} \geq 0.12 \quad R^2 = 0.98 \end{cases}, \qquad [6]$$

303
$$\begin{cases} c = -12.57 f_{sa} + 6.32 & f_{sa} \leq 0.40 \quad R^2 = 0.99 \\ c = 8.52 f_{sa} - 2.28 & f_{sa} > 0.40 \quad R^2 = 0.99 \end{cases}. \qquad [7]$$

304 Parameter *b* was related to ρ_b and f_{sa} as they both affected the magnitude of the $\kappa(S_r)$
305 curve. The following relationship was established by applying a multiple regression

306 algorithm that was included in the Data Analysis of Microsoft EXCEL (version 14 for
307 Windows) to the b, ρ_b and f_{sa} values listed in Table 2,

308
$$\begin{cases} b = 5.06 + 5.22\, f_{sa}\rho_b - 8.73\, f_{sa} & f_{sa} \le 0.40 \quad R^2 = 0.99 \\ b = 3.82 + 1.38\, f_{sa}\rho_b - 0.56\, f_{sa} & f_{sa} > 0.40 \quad R^2 = 0.99 \end{cases}. \qquad [8]$$

309 Thus, when f_{sa}, f_{cl}, and ρ_b data are available, the $\kappa(S_r)$ function can be estimated
310 directly by using Eqs. [5-8].

311 **4. Model validation**

312 We evaluated the performance of the new κ model (Eqs. [5-8]) by using published
313 datasets on both coarse-textured and fine-textured soils covering wide ranges of S_r and ρ_b.
314 For each soil, parameters a, b, and c were determined from measured f_{sa}, f_{cl}, and ρ_b values
315 using Eqs. [6-8]. Then κ values were estimated using Eq. [5]. The RMSE and bias of the
316 κ estimations were used to indicate model performance,

317
$$\mathrm{RMSE} = \sqrt{\frac{\sum\left(\kappa_{mea} - \kappa_{est}\right)^2}{n}}, \qquad [9]$$

318
$$\mathrm{bias} = \frac{\sum\left(\kappa_{mea} - \kappa_{est}\right)}{n}. \qquad [10]$$

319 where n is the number of data points, κ_{mea} and κ_{est} represent the measured and estimated
320 κ values, respectively.

321 *4.1 Model evaluation using κ measurements on repacked soil samples*

322 Figure 4 presents the measured and estimated κ values as a function of S_r for a
323 coarse-textured soil and a fine-textured soil. Soil 10 was a sandy loam soil from Ochsner

et al. (2001) with ρ_b ranging from 0.95 to 1.69 g cm^{-3}, and Soil 11 was a clay loam soil from Ochsner et al. (2001) with ρ_b ranging from 0.85 to 1.52 g cm^{-3}. Both measured and estimated $\kappa(S_r)$ values showed the following characteristics: (1) a soil with a larger f_{sa} (i.e., Soil 10) had a higher κ_m at a specific S_r, and a sharper κ increase in the low S_r region (Fig. 4a), while a fine-textured soil (i.e., Soil 11) exhibited more gradual change in this region (Fig. 4b); (2) for a particular soil, a greater ρ_b produced a larger κ at a specific S_r. In general, the new model provided fairly good κ estimations for variations in S_r and ρ_b. The RMSE and bias values of κ estimates were within 0.75×10^{-7} m^2 s^{-1} and 0.54×10^{-7} m^2 s^{-1} on Soils 10 and 11, respectively (Table 3).

The κ model was also tested on one coarse-textured soil and four fine-textured soils (Soils 12 and 13 from Ochsner et al. 2001 and Soils 9, 14 and 15 from Liu et al. 2008b). The repacked soil columns covered a range of ρ_b conditions (Table 1). The κ estimates agreed closely with the measured values, as indicated by the random distribution of data points along the 1:1 line (Fig. 5), and the low RMSE (within 0.64×10^{-7} m^2 s^{-1}) and bias (from -0.39 to 0.45×10^{-7} m^2 s^{-1}) (Table 3). Thus, the new model provided accurate κ estimates on both coarse-textured and fine-textured soils over wide ranges of S_r and ρ_b.

4.2 Model evaluation using in situ κ measurements in tillage plots

Tillage practices alter soil thermal properties, heat transfer in soils and near surface microclimate mainly by changing soil ρ_b and θ. For the tillage study on Soil 16, θ varied from 0.22 to 0.33 cm^3 cm^{-3} and the range of ρ_b was 1.06 to 1.58 g cm^{-3}. In general, the

344 NT plot had larger θ and ρ_b values (Figs. 6a and 6b) in the 0- to 10-cm and 10- to 20-cm
345 soil layers, while the differences between CT and RT plots were not significant. As a
346 result, the measured and estimated κ values for the NT plot were larger than those for the
347 CT and RT plots (Fig. 6c).

348 Comparisons between measured and estimated κ showed that most of the data
349 distributed randomly along the 1:1 line, and about 80% of the data were within the 10%
350 error lines (Fig. 6d), with an RMSE of 0.54×10^{-7} m^2 s^{-1} and a bias of 0.27×10^{-7} m^2 s^{-1}
351 for all of the sampling locations. The new model well captured the κ variability in the
352 three tillage systems (Fig. 6c), and the κ estimates were consistent with the HP measured
353 values (Fig. 6d). For the CT treatment, κ was underestimated slightly (Fig. 6d). The
354 errors might come from: (1) κ measurement errors with the HP method due to the
355 presence of crop residue in the soil layer; (2) the point measurements of θ and ρ_b by core
356 sampling might not fully capture the field variability; (3) the proposed κ model ignores
357 soil structural changes caused by tillage practices. Kaune et al. (1993) observed larger
358 apparent κ values in structured soils than in disturbed soils; and (4) we ignored the
359 influences of SOM on κ. Zheng et al. (2015) reported that including SOM content as a
360 thermal property parameter in the Noah land surface model influenced λ estimates
361 significantly but had negligible effects on heat flux and temperature simulations. In this
362 study, the soil samples had SOM contents less than 3% (Table 1). Further study is
363 required to investigate the effects of SOM on κ for soils with high SOM contents (e.g.,

peats).

4.3 Prediction of near-surface soil temperature

In this section, we compare temperature measurements against values estimated with the harmonic method (Eqs. [1] and [2]) over a period of 7 days. The daily average θ, ρ_b and mineral fractions were used to estimate κ values (Eqs. [5-8]) of the 0- to 50-mm and 50- to 100-mm soil layers. For each day, we determined A_n and ϕ_n by fitting Eq. [1] to the observed soil temperatures at the 14-mm depth using a finite Fourier series with five harmonics (i.e., M = 5). The daily $\bar{T}$, A_n and ϕ_n values of the 14-mm depth, along with modeled κ for each day, were then used as inputs in Eq. [2] for estimating soil temperatures at soil depths of 26 mm and 66 mm. The κ values for the 14- to 66-mm soil layer were taken as the weighted averages of those values of the 0- to 50-mm and 50- to 100-mm soil layers.

Figure 7 presents the results of daily mean θ, κ estimates, the observed and fitted soil temperatures at the 14-mm depth, the net radiation, and the observed and estimated soil temperatures at the 26- and 66-mm depths during a rain-free period from DOY 258 to 264, 2014. During this period, κ varied mainly with θ, because ρ_b values changed little with time. Both θ and κ varied significantly with soil depth (Fig. 7a), i.e., greater θ and ρ_b values were observed at 60-mm than those at 20-mm, leading to a κ difference about 2.0 × 10^{-7} m^2 s^{-1} between the two depths. Under all climatic conditions (cloudy, partially cloudy and clear days, as indicated by the changes in net radiation), harmonic functions

384 successfully described diurnal soil temperature variations at the 14-mm depth (Fig. 7b).

385 The estimated soil temperatures at the 26- and 66-mm depths agreed well with the
386 observed values (Fig. 7c), with RMSEs of 0.61^{o}C and 0.58^{o}C for the 26- and 66-mm
387 depths, respectively. This suggested that the new model was capable of providing reliable
388 κ estimates when accurate ρ_b and θ data were available. Thus, the new κ model can be
389 used in heat conduction models to estimate the spatial and temporal patterns of
390 subsurface soil temperature. Further studies are required to evaluate the new κ model in
391 more complicated scenarios, e.g., heat transfer in soils with partial vegetation-cover, and
392 under conditions where latent and convective heat transfer become apparent. Dynamic
393 monitoring of ρ_b is also required where soil structure varies strongly over time.

394 *4.4 Potential limitations of the new model*

395 We demonstrated that the proposed $\kappa(S_r)$ model was capable of producing acceptable
396 κ data across the entire S_r range for soils with different textures and ρ_b. The deviation of
397 the modeled κ data from the measured κ values might come from several error sources.
398 First, we obtained parameters *a*, *b*, and *c* using PSD rather than soil mineralogical
399 information. Some studies have shown that using PSD instead of soil mineral
400 composition produces biased κ estimations for soils with high fractions of quartz
401 (Bristow 1998; Peters-Lidard et al. 1998; Lu et al. 2014). Second, our model ignores the
402 effects of soil temperature and soil structure on κ values, which merit further study. Third,
403 the κ measurements by the HP sensors are subject to errors associated with probe

404 deflection, imperfect probe-soil contact, and irregular ambient temperature changes (Liu
405 et al. 2017), which affect the accuracy of the measured κ values.

406 Equation [5] fails in situations where the soils are completely dry (i.e., $S_r = 0$). Based
407 on HP measurements on dry mineral soils, Lu et al. (2013) showed that the κ_{dry} values
408 varied within a small range of 2.18 to 2.58 × 10^{-7} m^2 s^{-1} with an average value of 2.41 ±
409 0.16 × 10^{-7} m^2 s^{-1} for a wide range of textures. Thus, it is recommended to assign a value
410 of 2.41 × 10^{-7} m^2 s^{-1} to κ_{dry} for dry soil samples. If c_s value is available, κ_{dry} can be
411 calculated using the following formula:

412 $$\kappa_{dry} = \frac{-0.56\tau + 0.51}{c_s}. \qquad [11]$$

413 **5. Summary and conclusions**

414 An empirical model for estimating κ from soil texture, ρ_b and S_r was developed, in
415 which the shape parameters *a*, *b* and *c* were obtained from f_{sa}, f_{cl} and ρ_b. Independent
416 evaluations of the model using published datasets on repacked soil samples as well as a
417 field measured dataset from a tillage experiment showed that the new model could
418 produce acceptable $\kappa(S_r)$ data across the entire S_r range. The model responded well to
419 variable ρ_b. The model estimated κ values were shown to be useful for estimating
420 near-surface soil temperature dynamics. These promising results indicated that the new κ
421 model could potentially be used in soil heat transfer models to make soil temperature and
422 heat flux estimations for meteorological and geophysical applications.

Acknowledgements

This research was supported by the National Natural Science Foundation of China (41671223), the National Key Technology Research and Development Program of China (2015CB150403), and the China Postdoctoral Science Foundation (2016M600148), the US Army Research Office (W911NF-16-1-0287), the US National Science Foundation (1623806), the USDA-NIFA multi-State Project 3188, by Hatch Act, and State of Iowa funds. We thank Dr. Sen Lu (Chinese Academy of Forestry), Dr. Tyson Ochsner (Oklahoma State University), Dr. Xiaoyang Peng (Sichuan Provincial Science and Technology Department), and Dr. Xiaona Liu (Taiyuan University of Science and Technology) for generously providing their experimental datasets.

References

Arkhangel'skaya, T.A., 2009: Parameterization and mathematical modeling of the dependence of soil thermal diffusivity on the water content. *Eurasian Soil Sci*., **42**, 162–172, doi:10.1134/S1064229309020070.

Bristow, K.L., 1998: Measurement of thermal properties and water content of unsaturated sandy soil using dual-probe heat-pulse probes. *Agric. For. Meteor*., **89**, 75–84, doi:10.1016/S0168-1923(97)00065-8.

Bristow, K.L., G.J. Kluitenberg, and R. Horton, 1994: Measurement of soil thermal properties with a dual-probe heat-pulse method. *Soil Sci. Soc. Amer. J*., **58**, 1288–1294, doi:10.2136/sssaj1994.03615995005800050002x.

443 Campbell, G.S., 1985: *Soil physics with BASIC: Transport models for soil–plant systems*.
444 Elsevier Sci. Publ. Co., New York, 150 pp.
445 Campbell, G.S., C. Calissendorff, and J.H. Williams, 1991: Probe for measuring soil
446 specific heat using a heat-pulse method. *Soil Sci. Soc. Amer. J.*, **55**, 291–293,
447 doi:10.2136/sssaj1991.03615995005500010052x.
448 Campbell, G.S., and J.M. Norman, 1998: *An introduction to environmental biophysics*.
449 2nd ed. Springer-Verlag, New York, 286 pp.
450 Carslaw, H.S., and J.C. Jaeger, 1959: *Conduction of heat in solids*. 2nd. Ed., Clarendon
451 Press, Oxford, 510 pp.
452 Chen, F., and J. Dudhia, 2001: Coupling an advanced land surface-hydrology model with
453 the Penn State-NCAR MM5 modeling system. Part I: model implementation and
454 sensitivity. *Mon. Wea. Rev.*, **129**, 569–585,
455 doi:10.1175/1520-0493(2001)129<0587:CAALSH>2.0.CO;2
456 de Silans, A.M.B.P., B.A. Monteny, and J.P. Lhomme, 1996: Apparent soil thermal
457 diffusivity, a case study: HAPEX-Sahel experiment. *Agric. For. Meteor.*, **81**,
458 201-216, doi:10.1016/0168-1923(95)02323-2.
459 de Vries, D. A., 1963: Thermal properties of soils. *Physics of plant environment*, W. R.
460 van Wijk, Ed., North-Holland Publ. Co., 210–235.
461 Evett, S.R., N. Agam, W.P. Kustas, P.D. Colaizzi, and R.C. Schwartz, 2012: Soil profile
462 method for soil thermal diffusivity, conductivity and heat flux: Comparison to soil

heat flux plates. *Adv. Water Resour*., **50**, 41–54, doi:10.1016/j.advwatres.2012.04.012.

Ewing, R., and R. Horton, 2007: Thermal conductivity of a cubic lattice of spheres with capillary bridges. *J. Phys. D*., **40**, 4959–4965, doi:10.1088/0022-3727/40/16/031.

Gao, Z.M., E.S. Russell, J.E.C. Missik, M.Y. Huang, X.Y. Chen, et al., 2017 (a): A novel approach to evaluate soil heat flux calculation: An analytical review of nine methods. *J. Geophys. Res-Atmos.*, **122,** 6934–6949, doi:10.1002/2017JD027160.

Gao, Z.Q., B. Tong, R. Horton, A. Mamtimin, Y.B. Li, and L.L. Wang, 2017 (b): Determination of desert soil apparent thermal diffusivity using a conduction-convection algorithm. *J. Geophys. Res*., **122**, 9569–9578, doi:10.1002/2017JD027290.

Gee, G.W., and D. Or, 2002: Particle-size analysis. *Methods of soil analysis: Part 4, Physical methods,* J. H. Dane and G. C. Topp, Eds., Soil Sci. Soc. Amer., 255–293.

Guan, X.D., J.P. Huang, N. Guo, J.R. Bi, and G.Y. Wang, 2009: Variability of soil moisture and its relationship with surface albedo and soil thermal parameters over the Loess Plateau. *Adv. Atmos. Sci*., **26**, 692–700, doi: 10.1007/s00376-009-8198-0.

Heusinkveld, B.G., A. Jacobs, A. Holtslag, and S.M. Berkowicz, 2004: Surface energy balance closure in an arid region: role of soil heat flux. *Agric. For. Meteor*., **122**, 21-37, doi:10.1016/j.agrformet.2003.09.005.

Horton, R., P.J. Wierenga, and D.R. Nielsen, 1983: Evaluation of methods for

determining the apparent thermal diffusivity of soil near the surface. *Soil Sci. Soc. Amer. J.*, **47**, 25-32, doi:10.2136/sssaj1983.03615995004700010005x.

Horton, R, 2002: Soil Thermal Diffusivity. *Methods of soil analysis: Part 4. Physical methods,* J. H. Dane and G. C. Topp, Eds., Soil Sci. Soc. Amer., 349–360.

Holmes, T.R.H., M. Owe, R.A.M. De Jeu, and H. Kooi, 2008: Estimating the soil temperature profile from a single depth observation: A simple empirical heat flow solution. *Water Resour. Res*., **44**, W02412, doi:10.1029/2007WR005994.

Jackson, R.D., and S.A. Taylor, 1986: Thermal conductivity and diffusivity. *Methods of soil analysis: Part 1. Physical and Mineralogical Properties, Including Statistics of Measurement and Sampling.* C.A. Black, Ed., Amer. Soc. Agron. and Soil Sci. Soc. Amer., 945–956.

Johansen, O., 1975: Thermal conductivity of soils. Ph.D. thesis, University of Trondheim, 236 pp.

Kaune, A., T. Türk, and R. Horn, 1993: Alteration of soil thermal properties by structure formation. *J. Soil Sci.*, **44**, 231–249, doi: 10.1111/j.1365-2389.1993.tb00448x.

Kluitenberg, G.J., K.L. Bristow, and B.S. Das, 1995: Error analysis of heat pulse method for measuring soil heat capacity, diffusivity, and conductivity. *Soil Sci. Soc. Amer. J.*, **59**, 719–726, doi:10.2136/sssaj1995.03615995005900030013x.

Koch, J., A. Siemann, S. Stisen, and J. Sheffield, 2016: Spatial validation of large scale land surface models against monthly land surface temperature patterns using

innovative performance metrics. *J. Geophys. Res-Atmos.*, **121**, 5430-5452, doi: 10.1002/2015JD024482.

Kodikara, J., P. Rajeev, and N.J. Rhoden, 2011: Determination of thermal diffusivity of soil using infrared thermal imaging. *Can. Geotech. J.*, **48**, 1295–1302, doi:10.1139/T11-036.

Lettau, H., 1954: Improved models of thermal diffusion in the soil. *Trans. Am. Geophys. Union.*, **35**, 121-132, doi: 10.1029/TR035i001p00121.

Liu, G., Y.L. Lu, M.M. Wen, T.S. Ren, and R. Horton, 2017: Advances in the heat-pulse technique: improvements in measuring soil thermal properties. *Methods of Soil Analysis*, Vol 2, Soil Sci. Soc. Amer., Madison, WI. doi:10.2136/msa2015.0028.

Liu, H.Z., B.M. Wang, and C.B. Fu, 2008(a): Relationships between surface albedo, soil thermal parameters and soil moisture in the semi-arid area of Tongyu, northeastern China. *Adv. Atmos. Sci*., **25**, 757–764, doi: 10.1007/s00376-008-0757-2.

Liu, X.N., T.S. Ren, and R. Horton, 2008(b): Determination of soil bulk density with thermo-time domain reflectometry sensors. *Soil Sci. Soc. Amer. J*., **72**, 1000–1005, doi:10.2136/sssaj2007.0332.

Lu, S., T.S. Ren, Y.S. Gong, and R. Horton, 2007: An improved model for predicting soil thermal conductivity from water content at room temperature. *Soil Sci. Soc. Amer. J*., **71**, 8–14, doi:10.2136/sssaj2006.0041.

Lu, Y.L., S. Lu, R. Horton, and T.S. Ren, 2014: An empirical model for estimating soil

thermal conductivity from texture, water content, and bulk density. *Soil Sci. Soc. Amer. J*., **78**, 1859-1868, doi:10.2136/sssaj2014.05.0218.

Lu, Y.L., X.N. Liu, M. Zhang, J.L. Heitman, R. Horton, and T.S. Ren. 2017: Thermo–time domain reflectometry method. Advances in monitoring in situ soil bulk density. *Methods of Soil Analysis*, Vol. 2, Soil Sci. Soc. Amer., Madison, WI. doi:10.2136/msa2015.0031.

Lu, Y.L., Y.J. Wang, and T.S. Ren, 2013: Using late time data improves the heat–pulse method for estimating soil thermal properties with the pulsed infinite line source theory. *Vadose Zone J*., **12**, doi: 10.2136/vzj2013.01.0011.

McCumber, M.C., and R.A. Pielke, 1981: Simulation of the effects of surface fluxes of heat and moisture in a mesoscale numerical model 1. Soil layer. *J. Geophys. Res*., **86**, 9929–9938, doi: 10.1029/JC086iC10p09929.

Nassar, I.N., and R. Horton, 1989: Determination of the apparent thermal diffusivity of a nonuniform soil. *Soil Sci*., **147**, 238–244, doi: 10.1097/00010694-198904000-00002.

Nassar, I.N., and R. Horton, 1990: Determination of soil apparent thermal diffusivity from multiharmonic temperature analysis for nonuniform soils. *Soil Sci*., **149**, 125–130, doi: 10.1097/00010694-199003000-00001.

Nelson, D.W., and L.E. Sommers, 1996: Total carbon, organic carbon, and organic matter. *Methods of soil analysis: Part. 3, Chemical Methods*, D.L. Sparks et al., Eds. Amer. Soc. Agron. and Soil Sci. Soc. Amer., 961-1010, doi:10.2136/sssabookser5.3.c34.

543 Nerpin, S.V., and A.F. Chudnovskii, 1967: *Physics of the soil*. Israel Program for
544 Scientific Translations. Keter Press, Jerusalem, 317 pp.
545 Ochsner, T.E., R. Horton, and T.S. Ren, 2001: A new perspective on soil thermal
546 properties. *Soil Sci. Soc. Amer. J.*, **65**, 1641–1647, doi:10.2136/sssaj2001.1641.
547 Peng, X., J. Heitman, R. Horton, and T.S. Ren, 2017: Determining near-surface soil heat
548 flux density using the gradient method: A thermal conductivity model-based
549 approach. *J. Hydrometeor*., **18**, 2285-2295, doi:10.1175/JHM-D-16-0290.1.
550 Peters-Lidard, C.D., E. Blackburn, X. Liang, and E.F. Wood, 1998: The effect of soil
551 thermal conductivity parameterization on surface energy fluxes and temperature. *J.*
552 *Atmos. Sci.*, **55**, 1209–1224, doi:
553 10.1175/1520-4930469(1998)055<1209:TEOSTC>2.0.CO;2.
554 Ren, T.S., K. Noborio, and R. Horton, 1999: Measuring soil water content, electrical
555 conductivity and thermal properties with a thermo-time domain reflectometry probe.
556 *Soil Sci. Soc. Amer. J.*, **63**, 450-457, doi:
557 10.2136/sssaj1999.03615995006300030005x.
558 Richtmeyer, R.D., and K.W. Morton, 1967: *Difference methods for initial-value problems*.
559 (2nd ed). Interscience Publishers, New York, 420 pp.
560 Ross, P.J., 2013: Estimation of nonuniform soil thermal properties by harmonic analysis.
561 *Vadose Zone J*., **12**, doi:10.2136/vzj2013.03.006.
562 Roxy, M.S., V.B. Sumithranand, and G. Renuka, 2014: Estimation of soil moisture and its

563 effect on soil thermal characteristics at Astronomical Observatory,
564 Thiruvananthapuram, south Kerala. *J. Earth Syst. Sci*., **123**, 1793-1807, doi:
565 10.1007/s12040-014-0509-x.
566 Seemann, J., 1979: Measuring technology. J. Seemann et al. (ed). *Agrometeorology*.
567 Springer-Verlag, Berlin., 40-50.
568 Van Wijk, W.R., and D.A. de Vries, 1963: *Physics of plant environment*. Periodic
569 temperature variations in a homogeneous soil. W.R. van Wijk (ed.) North-Holland
570 Publ. Co., 102-143.
571 Wang, K.G., P.C. Wang, J.M. Liu, M. Sparrow, S. Haginoya, and X.J. Zhou, 2005:
572 Variation of surface albedo and soil thermal parameters with soil moisture content at
573 a semidesert site on the western Tibetan Plateu. *Bound.-Layer Meteor*., **116**, 117–
574 129, doi:10.1007/s10546-004-7403-z.
575 Wang, Z.H., and E. Bou-Zeid, 2012: A novel approach for the estimation of soil ground
576 heat flux. *Agric. For. Meteor*., **154–155**, 214–221, doi:
577 10.1016/j.agrformet.2011.12.001.
578 Welch, S.M., G.J. Kluitenberg, and K.L. Bristow, 1996: Rapid numerical estimation of
579 soil thermal properties for a broad class of heat-pulse emitter geometries. *Meas. Sci.*
580 *Technol*., **7**, 932–938, doi:10.1088/0957-0233/7/6/012.
581 Wierenga, P.J., D.R. Nielsen, and R.M. Hagan, 1969: Thermal properties of a soil based
582 upon filed and laboratory measurements. *Soil Sci. Soc. Amer. Proc*., **33**, 354-360,

583 doi:10.2136/sssaj1969.03615995003300030009x.

584 Wolfram, S., 2003: *The Mathematica book*. 5th ed. Wolfram Media, Champaign, IL, 1488

585 pp.

586 Xia, Y., M. Ek, J. Sheffield, B. Livneh, M. Huang, H. Wei, and E. Wood, 2013: Validation

587 of Noah-simulated soil temperature in the North American land data assimilation

588 system phase 2. *J. Appl. Meteor. Climatol.*, **52**, 455-471, doi:

589 10.1175/JAMC-D-12-033.1.

590 Zheng, D.H., R. van der Velde, Z.B. Su, X. Wang, J. Wen, M.J. Booij, A.Y. Hoekstra, and

591 Y.Y. Chen, 2015: Augmentations to the Noah Model Physics for Application to the

592 Yellow River Source Area. Part II: Turbulent Heat Fluxes and Soil Heat Transport. *J.*

593 *Hydrometeor*., **16**, 2677-2694.

TABLE 1. Soil particle size distribution, soil organic matter (SOM) content, and bulk density (ρ_b) for 16 soils used in the study. Soils 1-8, 16 are new measurements, and Soils 9-15 are from the literature.

Soil ID	Texture	Particle size distribution			SOM	ρ_b	Source
		2-0.05 mm	0.05-0.002 mm	<0.002 mm			
		(%)			(%)	(g cm^{-3})	
1	Sand	94	1	5	0.09	1.60	This study
2	Loamy sand	79	13	8	0.18	1.28/1.49	This study
3	Sandy loam	67	21	12	0.86	1.39	This study
4	Loam	50	41	9	0.25	1.38	This study
5	Loam	40	49	11	0.49	1.30	This study
6	Clay loam	32	38	30	0.27	1.29	This study
7	Silt loam	27	51	22	1.19	1.33	This study
8	Silt loam	19	54	27	0.39	1.30	This study
9	Sand	93	0	7	0.06	1.40-1.60	Liu et al. (2008b)
10	Sandy loam	66	23	11	2.30	0.95-1.69	Ochsner et al. (2001)
11	Clay loam	37	35	28	2.30	0.85-1.52	Ochsner et al. (2001)
12	Silt loam	23	64	13	0.90	0.91-1.45	Ochsner et al. (2001)
13	Silt clay loam	12	56	32	1.10	1.05-1.47	Ochsner et al. (2001)
14	Clay loam	31	39	30	0.27	1.06-1.26	Liu et al. (2008b)
15	Silt loam	15	65	20	1.46	1.12-1.38	Liu et al. (2008b)
16	Silt loam	17	62	21	1.10	1.06-1.58	This study

TABLE 2. The ranges of degree of saturation (S_r), model parameters *a*, *b* and *c*, and root mean square errors (RMSE) of the new model on Soils 1-8. The model parameters and RMSEs were obtained by fitting Eq. [5] to heat-pulse thermal diffusivity vs. S_r data with a nonlinear regression algorithm (Wolfram, 2003).

Soil ID	S_r range	*a*	*b*	*c*	RMSE (10^{-7} m^2 s^{-1})
1	0.06–1	0.20	5.35	5.45	0.20
2	0.02–0.46	0.26	4.75	5.08	0.34
2	0.02–0.64	0.32	4.99	4.42	0.33
3	0.03–0.89	0.30	4.79	3.16	0.25
4	0.03–0.95	0.36	4.52	1.74	0.35
5	0.03–0.89	0.37	4.27	1.28	0.27
6	0.08–1	0.46	4.47	2.38	0.29
7	0.05–0.97	0.40	4.58	2.82	0.31
8	0.08–0.96	0.42	4.68	3.96	0.21

TABLE 3. The root mean square errors (RMSE) and bias of the new model for estimating soil thermal diffusivity on Soils 9-16 with various bulk densities and degree of saturation (S_r).

Soil ID	S_r range	RMSE (10^{-7} m^2 s^{-1})	bias (10^{-7} m^2 s^{-1})
9	0.02–0.50	0.64	0.21
10	0.19–0.95	0.75	0.64
11	0.19–0.88	0.54	0.29
12	0.03–0.43	0.33	0.11
13	0.08–0.64	0.61	0.45
14	0.06–0.48	0.53	0.36
15	0.06–0.52	0.64	-0.39
16	0.40–0.78	0.54	0.27

Figure Caption List

FIG. 1. Measured (symbols) and fitted (curves) thermal diffusivity (κ) vs. degree of saturation (S_r) for eight soils of various textures. The curves were obtained by fitting Eq. [5] to the measured $\kappa(S_r)$ using a nonlinear curve fitting method (Wolfram, 2003). The fitted equations are presented in the figure.

FIG. 2. The effects of (1) parameter *a*, (2) parameter *b*, and (3) parameter *c* on soil thermal diffusivity (κ)–degree of saturation (S_r) curves obtained with Eq. [5]. The presented curves have assigned values for parameters *a*, *b* and *c*.

FIG. 3. Dependence of (1) parameter *a* on clay fraction (f_{cl}), and parameters (2) *b* and (3) *c* on sand fraction (f_{sa}) for Soils 1-8. The symbols represent the fitted *a*, *b* and *c* results in Table 2. The lines are the linear regression results for each domain.

FIG. 4. Measured and estimated soil thermal diffusivity (κ) vs. degree of saturation (S_r) data with the new model for coarse-textured Soil 10 (sand fraction $f_{sa} > 0.40$) (a) and fine-textured Soil 11 ($f_{sa} \leq 0.40$) (b). The repacked soil bulk density (ρ_b) ranges are presented in the figure.

FIG. 5. Measured and estimated thermal diffusivity (κ) using the new model for coarse-textured Soil 9 (sand fraction $f_{sa} > 0.40$) and fine-textured Soils 12-15 ($f_{sa} \leq 0.40$). The solid line is a 1:1 line, and the dashed lines are the 10% error lines.

FIG. 6. The (a) measured soil water content (θ), (b) bulk density (ρ_b), (c) measured soil thermal diffusivity (κ), (d) comparisons between estimated κ with the new model and the in situ measured values for the 0- to 10-cm and 10- to 20-cm soil layers in conventional tillage (CT), rotary tillage (RT), and no tillage (NT) treatment plots,

626 respectively. The bars represent standard deviations of each value.

627 FIG. 7. Daily mean soil water content (θ) and the estimated soil thermal diffusivity (κ)
628 with the new model for the 20- and 60-mm depths (a); Net radiation, observed and
629 fitted (Eq. [1]) soil temperatures at 14-mm depth (b); and observed and estimated (Eq.
630 [2]) soil temperatures at 26- and 66-mm depths (c) during Day of Year 258 to 264,
631 2014.

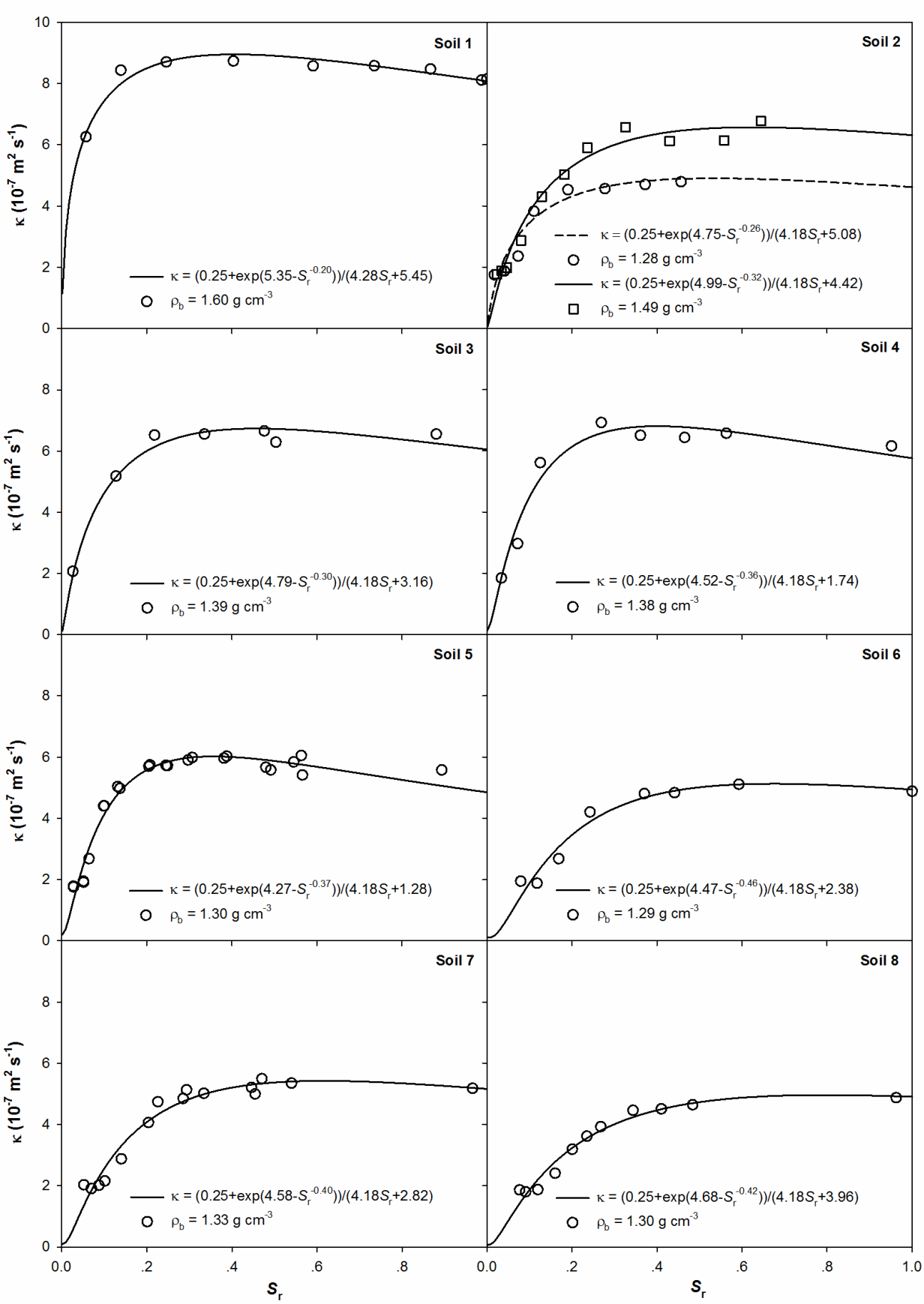

632

633 FIG. 1. Measured (symbols) and fitted (curves) thermal diffusivity (κ) vs. degree of saturation (S_r) for

634 eight soils of various textures. The curves were obtained by fitting Eq. [5] to the measured κ(S_r) using a

635 nonlinear curve fitting method (Wolfram, 2003). The fitted equations are presented in the figure.

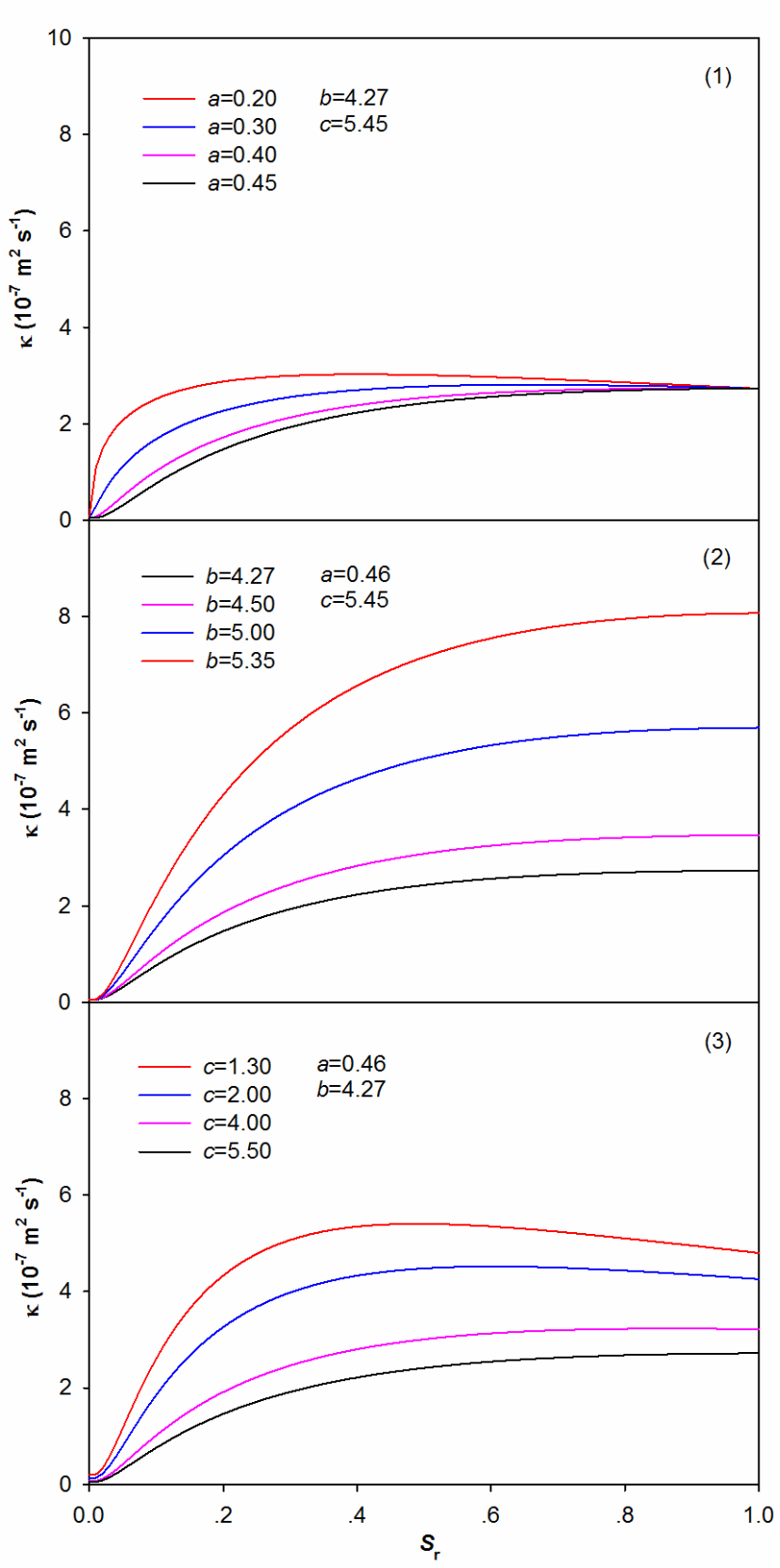

636

637 FIG. 2. The effects of (1) parameter *a*, (2) parameter *b*, and (3) parameter *c* on soil thermal diffusivity

638 (κ)–degree of saturation (S_r) curves obtained with Eq. [5]. The presented curves have assigned values

639 for parameters *a*, *b* and *c*.

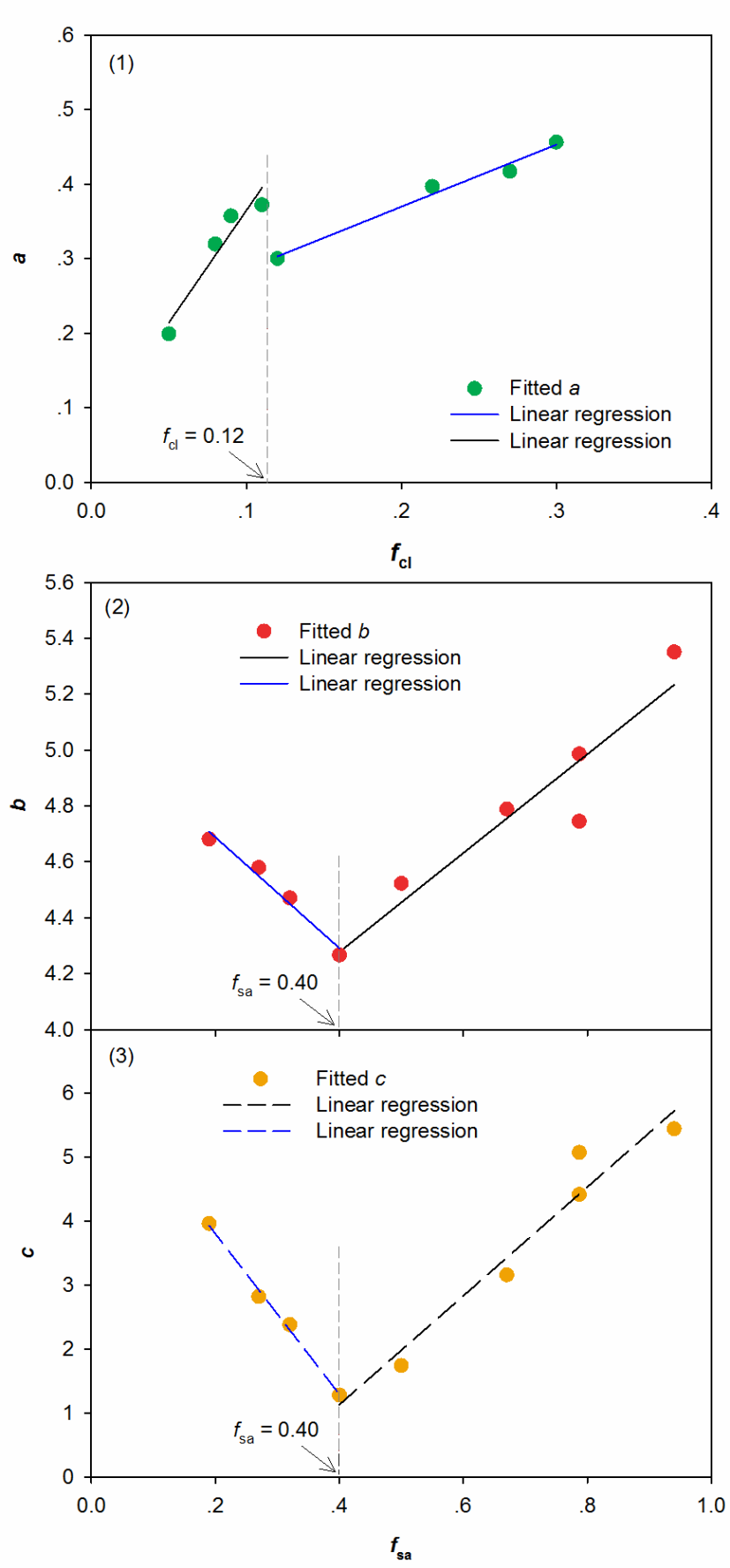

640

641 FIG. 3. Dependence of (1) parameter *a* on clay fraction (f_{cl}), and parameters (2) *b* and (3) *c* on sand

642 fraction (f_{sa}) for Soils 1-8. The symbols represent the fitted *a*, *b* and *c* results in Table 2. The lines are

643 the linear regression results for each domain.

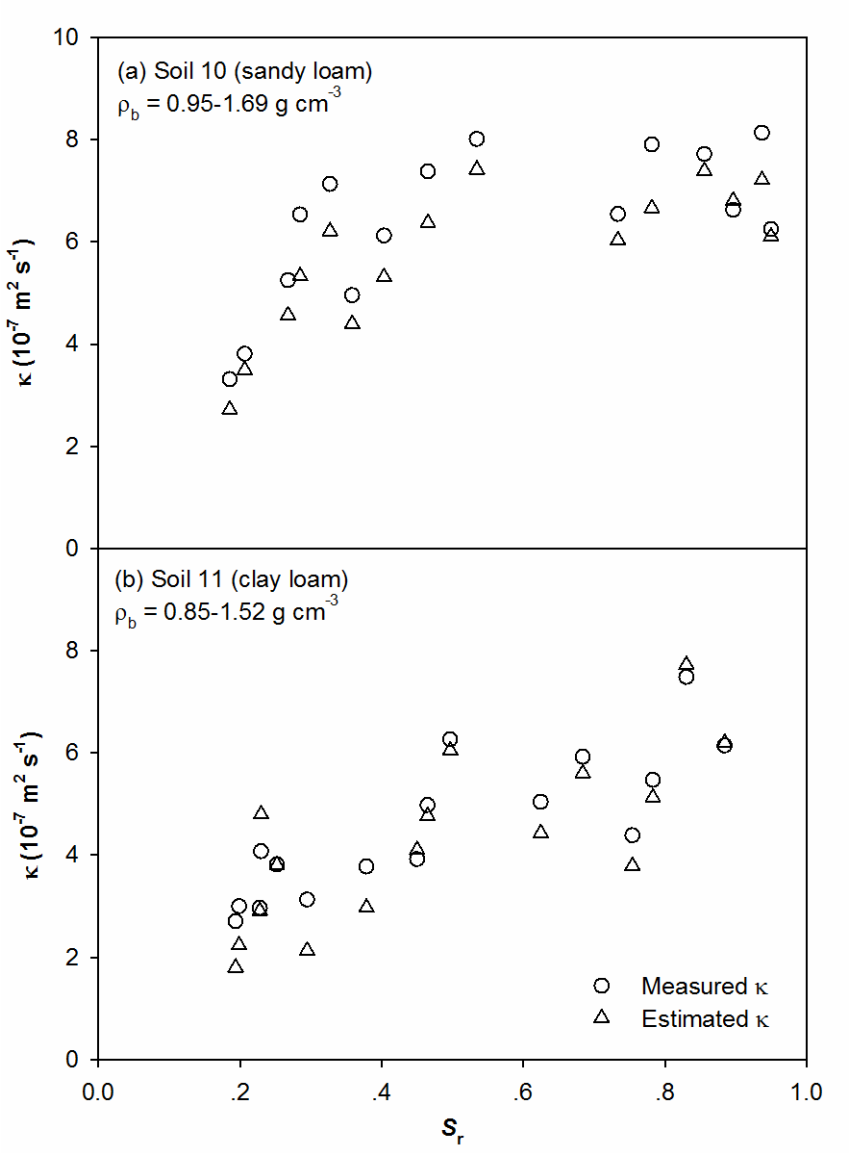

644

645 FIG. 4. Measured and estimated soil thermal diffusivity (κ) vs. degree of saturation (S_r) data with the

646 new model for coarse-textured Soil 10 (sand fraction $f_{sa} > 0.40$) (a) and fine-textured Soil 11 ($f_{sa} \leq 0.40$)

647 (b). The repacked soil bulk density (ρ_b) ranges are presented in the figure.

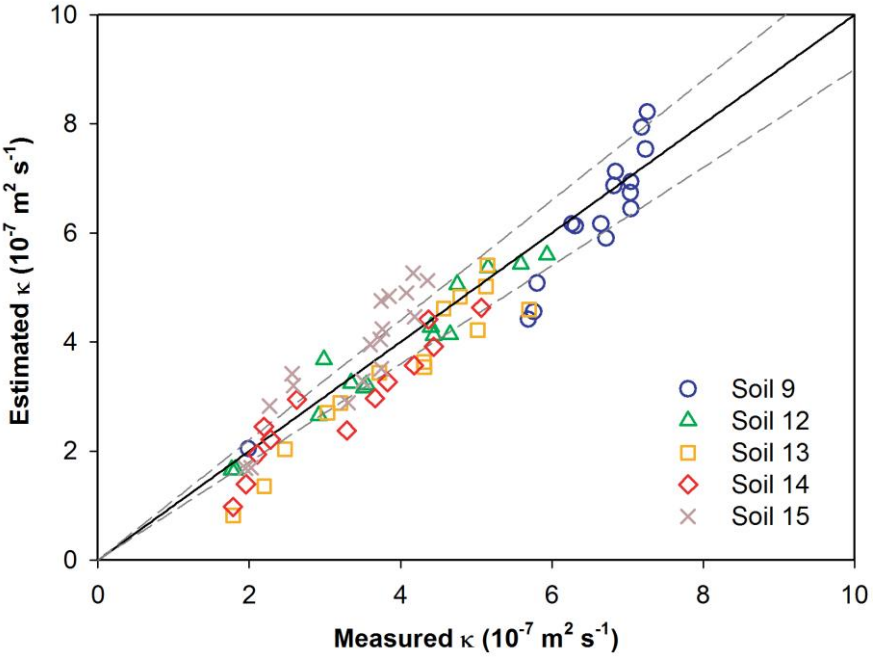

FIG. 5. Measured and estimated thermal diffusivity (κ) using the new model for coarse-textured Soil 9 (sand fraction $f_{sa} > 0.40$) and fine-textured Soils 12-15 ($f_{sa} \leq 0.40$). The solid line is a 1:1 line, and the dashed lines are the 10% error lines.

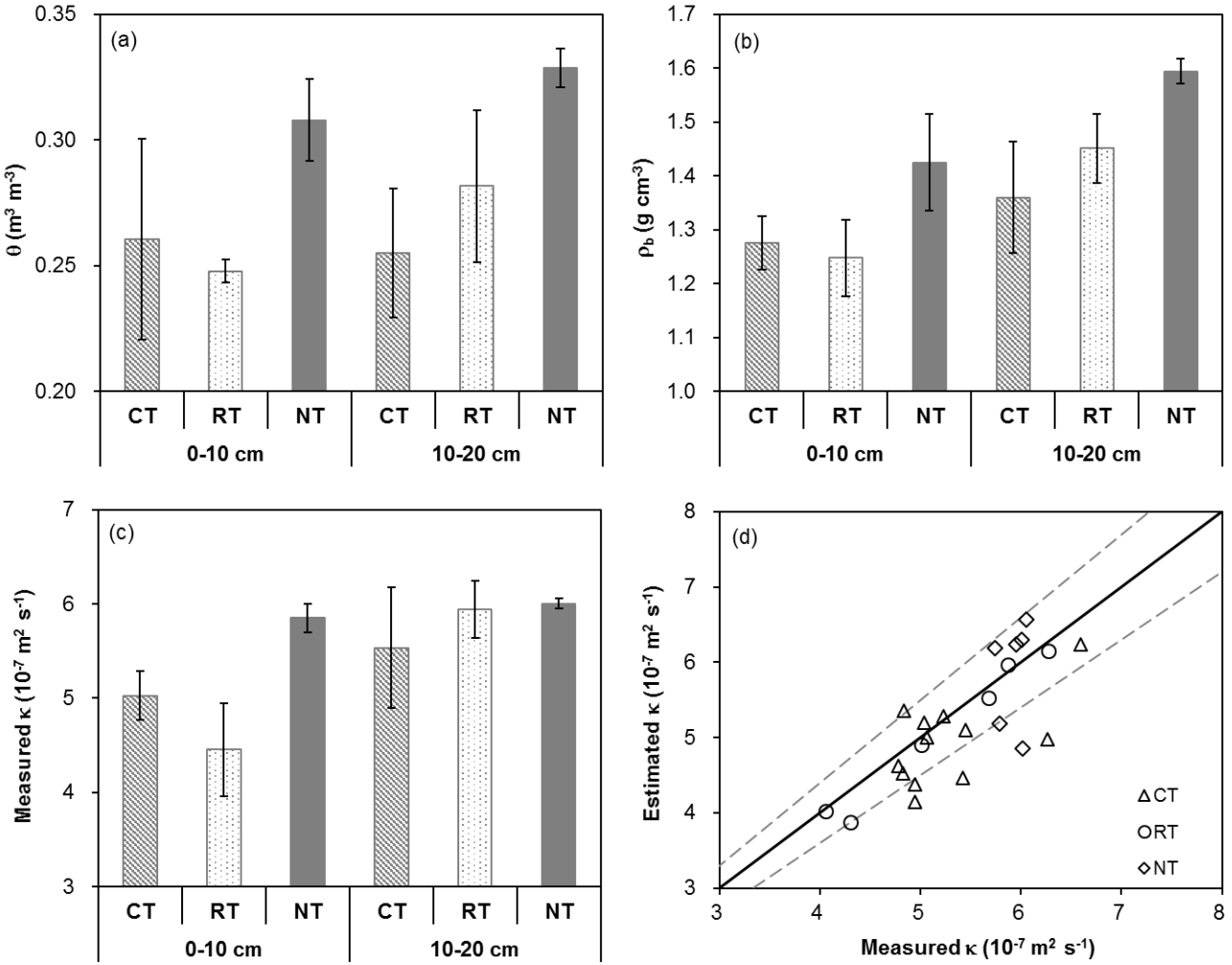

652

653 FIG. 6. The (a) measured soil water content (θ), (b) bulk density (ρ_b), (c) measured soil thermal diffusivity (κ), (d) comparisons between

654 estimated κ with the new model and the in situ measured values for the 0- to 10-cm and 10- to 20-cm soil layers in conventional tillage (CT),

655 rotary tillage (RT), and no tillage (NT) treatment plots, respectively. The bars represent standard deviations of each value.

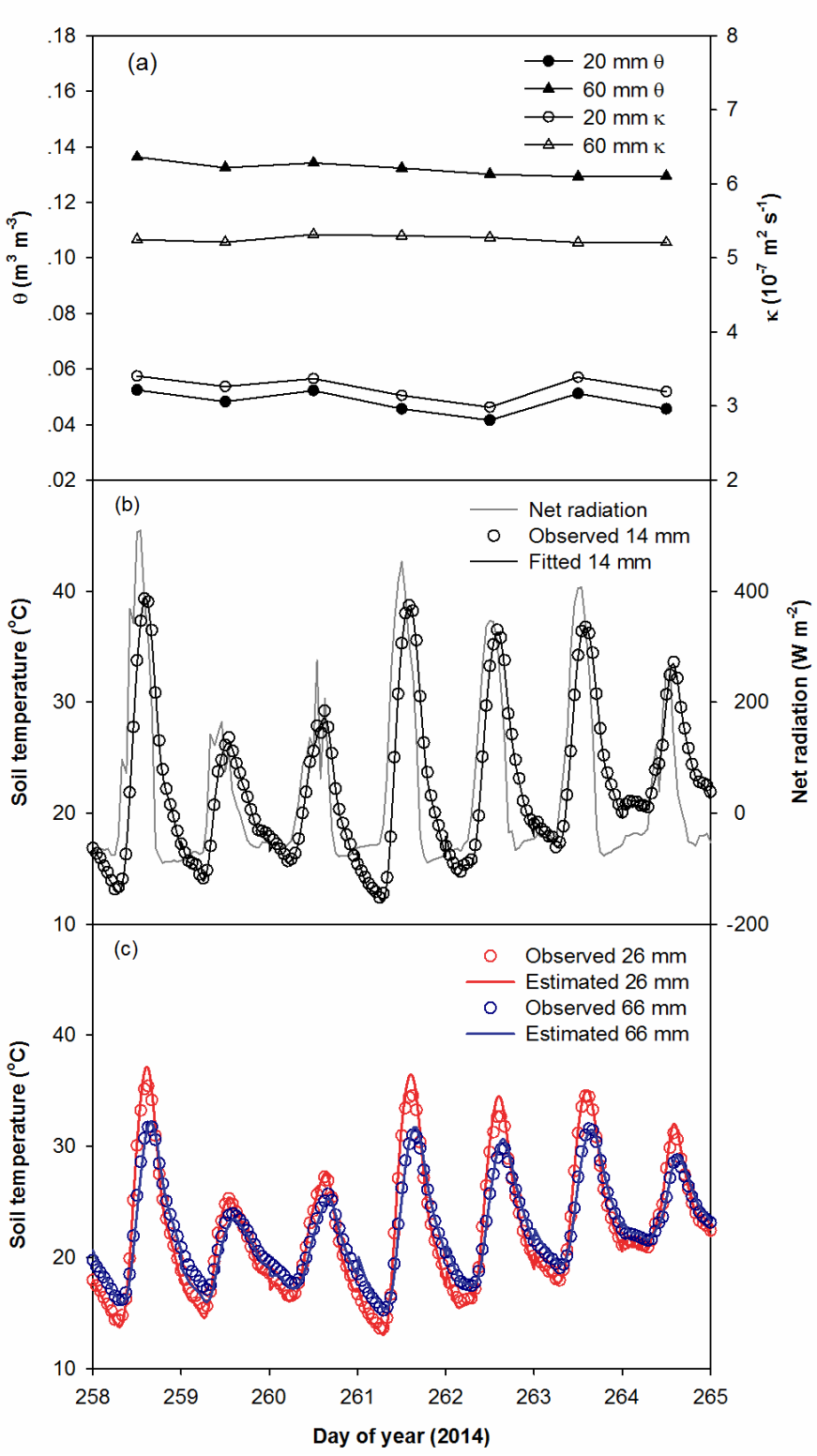

656

657 FIG. 7. Daily mean soil water content (θ) and the estimated soil thermal diffusivity (κ)

658 with the new model for the 20- and 60-mm depths (a); Net radiation, observed and

659 fitted (Eq. [1]) soil temperatures at 14-mm depth (b); and observed and estimated (Eq.

660 [2]) soil temperatures at 26- and 66-mm depths (c) during Day of Year 258 to 264,

661 2014.